ELSEVIER

Catalysis Today 48 (1999) 185–194

CATALYSIS TODAY

Improving conversion and selectivity of catalytic reactions in bubbling gas–solid fluidized bed reactors by control of the nonlinear bubble dynamics

Sander Kaart*, Jaap C. Schouten[1], Cor M. van den Bleek

Department of Chemical Process Technology, Delft University of Technology, Julianalaan 136, 2628 BL Delft, Netherlands

Abstract

In this paper a model is presented that is a dynamic extension of the classic two-phase reactor models used to predict conversion and selectivity of fluidized reactors. The most important part of the model is a dynamic discrete bubble model that can correctly predict bubble sizes and also exhibits chaotic dynamics. This bubble model is based on the discrete bubble models presented by Clift and Grace [AIChE Symp. Ser. 66 (105) (1970) 14; 67 (116) (1971) 23; in: J.F. Davidson, R. Clift, D. Harrison (Eds.), Fluidization, Academic Press, London, 1985, p. 73] and Daw and Halow [AIChE Symp. Ser. 88 (289) (1992) 61]. The latter showed that this type of models can exhibit chaotic behavior. By application of an extended version of Pyragas' control algorithm [K. Pyragas, Phys. Lett. A 170 (1992) 421] the bubble dynamics can be changed from chaotic to periodic in a 'flow'-regime in which the model otherwise would predict chaotic behavior. Pyragas' control algorithm is used to synchronize a chaotic system with one of its periodic solutions using a feedback control loop. This results in smaller bubbles, thus enhancing mass transfer of the reactant gas in the bubbles to the catalyst particles. The model is used to predict the effect of the changed bubble dynamics on a catalytic reaction of industrial importance, viz. the ammoxidation of propylene to acrilnitril (Sohio process). It is shown that both conversion and selectivity are appreciably enhanced.

Keywords: Fluidization; Chaos control; Selectivity; Bubble model

1. Introduction

In chemical reactor engineering there is a strong need for an integrated approach in the development of new reactors as well as in the optimization of conventional reactor designs [1,2]. Here a strong interaction takes place with the field of catalysis leading to new catalyst shapes and so-called structured catalytic reactors in which the arrangement of the catalyst in the reactor is optimized with respect to e.g. mass transfer and reactor pressure drop [3]. In general, the integrated approach in reactor design aims at operating the reactor at its thermodynamic, kinetic, and mass and heat transfer limits in order to optimize conversion and selectivity. This may lead to designs in which different functions are combined, e.g. integration of catalysis, reactant and product separation, heat input and transfer [4]. In general, the functioning of the reactor will also strongly depend on flow pattern, for example in

*Corresponding author.

[1]Present address: Eindhoven University of Technology, Laboratory of Chemical Reactor Engineering, P.O. Box 513, 5600 MB Eindhoven, The Netherlands.

0920-5861/99/$ – see front matter
PII: S0920-5861(98)00372-1

the complex geometries around the catalyst particles. Here computational fluid dynamics is a useful tool to evaluate the flow for optimization of the flow pattern. Also transient operation of the reactor may be highly advantegeous to integrate and optimize for example thermodynamics and heat transfer, as is illustrated by the use of periodic flow reversal in adiabatic fixed bed reactors [1,2,4].

In this paper, we will illustrate with a model study that transient operation may also improve conversion and selectivity of catalytic reactions in fluidized bed reactors through a decrease of the overall mass transfer resistance between bubble phase and the catalyst. This is achieved by exploiting the sensitivity of the chaotic bubble pattern in the reactor to small variations in the gas input flow containing the reactant. This study thus illustrates that there is clearly also room for improvement of the chemical performance of (conventional) multiphase reactors, like the fluidized bed, in which the flow is much more complex than in structured catalytic reactors.

It is well known that conversion in bubbling gas–solid fluidized bed reactors is generally lower than in fixed bed reactors with the same space velocity. The main reason for this poorer performance is found in the presence of bubbles. On the one hand, bubbles form an additional resistance to mass transfer between reactant gas and catalyst particles. On the other hand, bubbles usually have a high rise velocity, so little time is left for mass transfer. Both effects, which increase with increasing bubble size, lead to the unwanted bypass of reactants.

Selectivity of complex catalytic reactions usually depends on the mass transfer properties of the reactor in which the reaction takes place. Consider, e.g., a consecutive reaction (A→P→R), and suppose mass transfer to and from the catalyst particles is slow; conversion will generally be low and selectivity will be in favor of the unwanted product *R*. The selectivity of complex reactions in gas–solid fluidized bed reactors depends not only on catalyst properties, but to a large extent on the mass transfer properties (i.e., bubble size) of the fluidized bed as well. By changing the bubble dynamics (i.e., rate of bubble growth, bubble coalescence), both conversion and selectivity of mass-transfer-limited catalytic reactions in bubbling gas–solid fluidized reactors can be improved.

Various recent studies have indicated that gas–solid fluidized beds are chaotic systems [5,6]. This means that the evolution in time of characteristic hydrodynamic variables in fluidized beds, such as local voidage or pressure, can only be reliably predicted over a short period of time. However, the corresponding trajectories in state space will stay within a bounded region (the system's attractor), never exactly returning to the same position. Embedded in this attractor are infinitely many unstable periodic orbits of the system. This implies that the (nonlinear) dynamics of fluidized beds are very sensitive to small changes in fluidization conditions. For example, small changes in the type or rate of gas supply (i.e., initial bubble size) may lead to stabilization of one of the periodic trajectories of the system and thus to significantly different bubble patterns.

It was shown by Schouten et al. [5] that the rising and nonlinearly interacting gas bubbles (i.e., the bubble dynamics) in the fluidized bed are responsible for the observed chaotic behavior. Control of the chaotic bubble patterns therefore might be a possible way to decrease the average bubble size and, consequently, to improve chemical performance (i.e. conversion and selectivity). An advantage of applying specific chaos control methods is that the fluidized bed's high sensitivity to small changes can be exploited, viz., only small control actions (i.e. perturbations of the gas velocity) may be sufficient. This is in contrast with earlier attempts as are mentioned in literature to suppress the bubbles in the bed by high energy demanding techniques like vibration [7] or magnetic stabilization [21].

The study presented in this paper aims at illustrating the effect of stabilizing different bubble patterns on the chemical performance, by controlling a dynamic reactor model of a bubbling fluidized bed and by comparing the conversion, selectivity, and yield in both the controlled and uncontrolled situation.

2. The dynamic reactor model

In this section the dynamic reactor model will be introduced. The model is based on classic two-phase fluidized bed reactor models like those of, e.g., Orcutt et al. [8] and Kunii and Levenspiel [9]. The bubble phase in this type of models is usually described with an average bubble diameter or with a bubble size

relation that presents the bubble diameter as a function of the axial position in the reactor. In this paper this two-phase approach is used, however, the bubble phase is described using a *dynamic* discrete bubble model. This model is described in Section 2.1. Section 2.2 describes the emulsion phase and the mass transfer between bubble and emulsion phase.

2.1. Dynamic bubble model

The dynamic bubble model used in this study is based on the discrete bubble models as presented by Clift and Grace [10–12] and Daw and Halow [13]. The latter showed that this type of bubble models can exhibit chaotic behavior. Relations similar to those of Clift and Grace were used by Glicksman and Lord [14] to predict successfully the bubble size in a single chain of rising bubbles.

The dynamic bubble model is summarized in Fig. 1. It describes a one-dimensional chain of two-dimensional bubbles. Starting at the bottom of the bed, bubbles are injected into the reactor with a fixed frequency ($1/T_p$); they become part of the bubble chain, every time the bubble flow (F_b) becomes zero (at $t=I_oT_p$). So the initial bubble volume of each bubble equals $F_oI_oT_p$ (m^3).

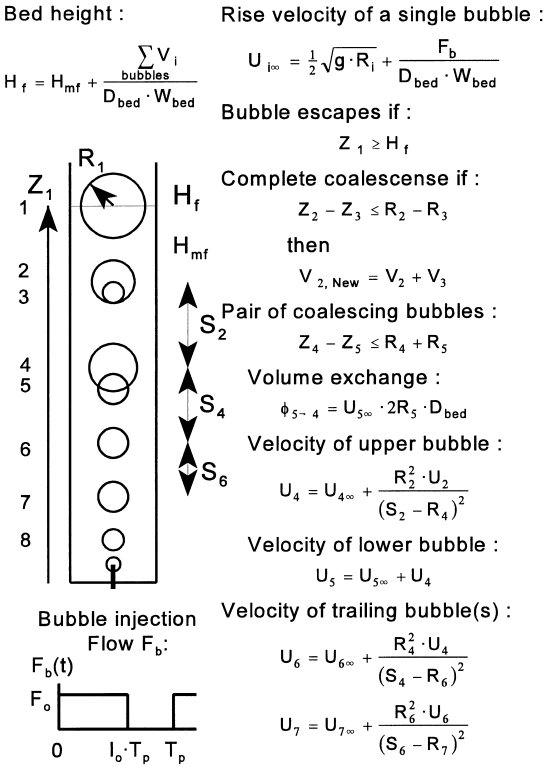

Fig. 1. Summary of the one-dimensional discrete bubble model.

As soon as the bubble detaches from the distributor, it obtains a velocity. This velocity has two components. First of all the bubble has its single bubble rise velocity U_∞. In addition to this, the bubble gets a velocity that depends on the distance *to* and size and velocity *of* the bubble above it. Fig. 1 shows some of the possible combinations. This velocity (the sum of both components) is integrated to give the bubble's position as a function of time.

When two or more bubbles touch, a coalescing pair (group) of bubble(s) is born. The lower bubbles in the group start to penetrate the bubbles directly above them, emptying themselves into the ones above them. The coalescence is said to be complete when the lower bubble completely penetrated the one above it. At that moment the lower bubble disappears and the remaining gas is added to the upper bubble. It is assumed that the gas exchange ($\phi_{i+1\to i}$) between two coalescing bubbles is proportional to the velocity difference between the two and proportional to the cross-sectional area of the lower bubble. Furthermore it is assumed that the velocity of the bubble following a group of coalescing bubbles is only affected by the bubble leading this group (or pair) of coalescing bubbles (Fig. 1).

A bubble leaves the reactor as soon as it reaches the bed level (H_f). The bed expansion ($H_f - H_{mf}$) is given by the total volume of bubbles in the bed and is thus time dependent.

To compare bubble sizes resulting from this model with the bubble size equation of Darton et al. [15], a number of simulations were done varying the bubble flow F_o to give excess gas velocities between 4.5 and 12 cm/s. The results are shown in Fig. 2. It is clear that the dynamic bubble model is able to predict bubble sizes that resemble those predicted by generally accepted bubble size relations like the one of Darton et al.

2.2. The mass transfer model

The first part of the dynamic reactor model is now available and gives a dynamic description of the bubble phase. The second part of the model will be

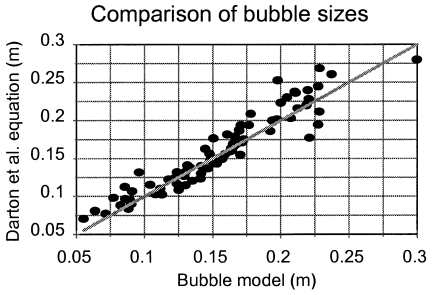

Fig. 2. Comparison of bubble sizes predicted with the dynamic bubble model and those predicted by the Darton et al. [15] equation for the same conditions.

described in this section. In the classic reactor models the emulsion phase is usually described by one of two common models. Some models assume the emulsion phase to be well mixed. Other models assume the minimum fluidization gas to flow in plug flow through the particulate phase. Based on these two extremes, the emulsion and bubble phase are contained in an arbitrary number of compartments, in this case seven, along the height of the bed; each compartment consists of two well-mixed reactors, one for the bubble phase and one for the emulsion phase (Fig. 3). Each compartment thus contains part of the emulsion and bubble phases; the fraction of emulsion or bubble phase per compartment is time-dependent. The six lower compartments have a fixed total volume and the top compartment has a variable volume. The bubble fraction is determined by the bubbles present between the upper and lower compartment boundaries. The amount of emulsion phase present in the compartments is determined by the volume not occupied by bubbles. Furthermore there are several flows of gas and solids going in and out of each compartment. A flow of bubble gas, determined by the bubble model, flows in and out of each compartment. Continuity demands an emulsion flow (viz., particles+gas) in and out of each compartment as well. Injection of bubbles induces an upward emulsion flow. Rising bubbles cause emulsion phase to flow downwards, filling the space previously occupied by the bubbles. The top compartment has a volume that is depending on the bed expansion; this means that the emulsion phase only enters and leaves the top compartment at its bottom. The flows of gas leaving the top of the upper compartment (and thus the reactor) are the bubble gas and emulsion gas flows.

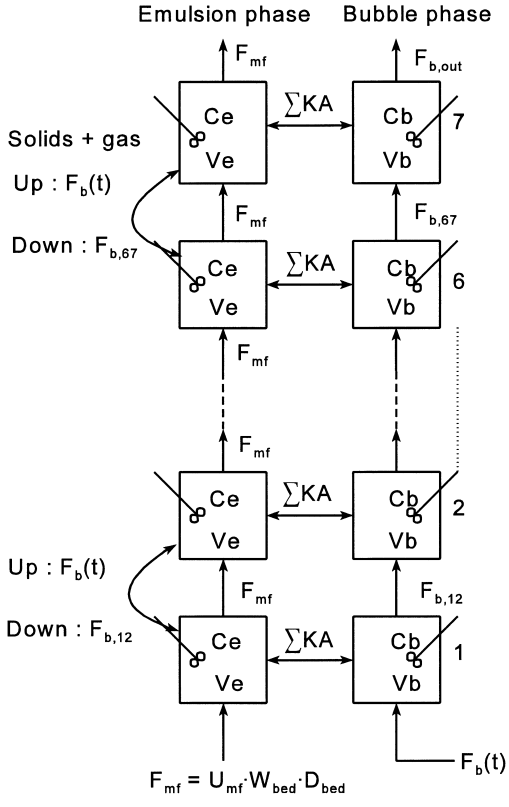

Fig. 3. Schematic representation of the mass transfer model.

To model mass transfer between the emulsion and bubble phases, each bubble has its own mass transfer coefficient (K) and mass transfer area (A), which are dependent on the bubble diameter. The mass transfer coefficient is based on the model given by Kunii and Levenspiel [9] and adjusted to account for two-dimensional bubbles. The transfer between bubble and emulsion phase in each compartment is determined by the sum of K times A for each bubble present in the compartment, and by the concentration difference between bubble and emulsion phase.

The combination of both the dynamic bubble model and the mass transfer model results in a dynamic version of a classic fluidized bed reactor model. Using this model it is possible to simulate the effect of changing bubble dynamics on the chemical performance of the fluidized bed. Daw and Halow [13] showed that a similar type of dynamic bubble model exhibits chaotic behavior, viz., when bubbles are injected with a certain rate, they do not leave the

reactor with a constant frequency but in a chaotic way. The dynamic bubble model described in this paper (Fig. 1) also shows chaotic behavior, as is indicated by finite, but non-zero values of the Kolmogorov entropy.

In the next section, the chaos control method used in this work will be explained.

3. Controlling chaotic systems

Chaos presents itself as irregular unpredictable motion and is often considered undesirable. Usually systems are operated well outside their chaotic regime, if possible, to avoid the unpredictable behavior. As mentioned before, this unpredictable behavior is caused by the strong sensitivity to small perturbations, characteristic for chaotic systems. Chaos control exploits this sensitivity and forces the system to follow some desired trajectory using only small control actions. In the past decade a number of possible control strategies is proposed in literature; see e.g. Kapitaniak [16] or Shinbrot [17] for reviews on this subject.

In this paper the method proposed by Pyragas [18] was used as a starting point and will be discussed in Section 3.1. In Section 3.2, the method is tailored to control the dynamic bubble model.

3.1. Pyragas' method

Pyragas' method is best explained using Fig. 4. The chaotic system (P) can be described by an unknown set of ordinary nonlinear differential equations of which some scalar variable (x) can be measured. Furthermore the system can be influenced by some external input. Using an adjustable feedback weight (K), the chaotic system (P) may be synchronized with an external oscillator (G). This oscillator is used to generate one of the unstable periodic orbits (UPOs) found in the system's output signal (x). A method of finding UPOs is looking for traces of signal for which $x(t)\approx x(t+T)$. An exact UPO should satisfy the condition $x(t)=x(t+T)$. Here T is the UPOs period. Now this trace of signal is used as a reference signal ($x(t)_{\mathrm{ref}}$), that is simulated by the oscillator. Pyragas used this method to successfully control the Rössler model [18].

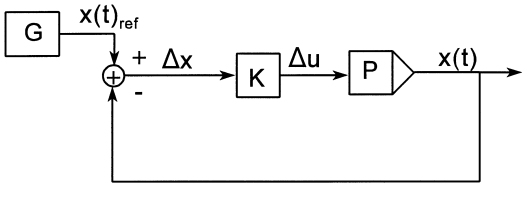

Fig. 4. Control scheme of Pyragas' method [18] to control (chaotic) dynamic systems.

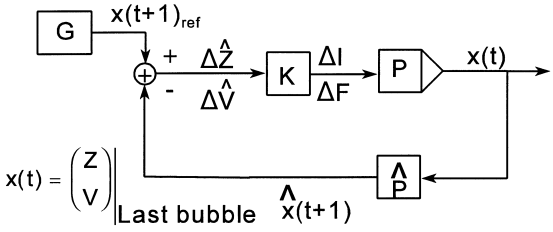

Fig. 5. Extended version of Pyragas' control scheme used to control the bubble model.

3.2. Controlling the bubble model

The control scheme introduced above is now further extended to control the dynamic bubble model (Fig. 5). First of all the state (i.e., the position (Z) and volume (V)) of the just detached bubble in the chain (no. 8 in Fig. 1) is chosen as the system's output signal ($x(t)$). This choice was made since the just detached bubble in the chain can directly be influenced by how it is introduced into the reactor. This automatically leads to the input available for external force: the input in the bubble model is the bubble injection flow $F_{\mathrm{b}}(t)$. For control purposes this flow is adjusted in two ways. First of all the maximum flow (F_{o}) is adjusted by adding a control action ΔF. Furthermore the 'on-fraction' (I_{o}) is adjusted by adding a control action ΔI. In this way the volume of the injected bubble can be controlled, as well as the moment at which the bubble is allowed to join the chain of rising bubbles above it. This way of forcing the system can also be implemented experimentally.

Since a bubble can only be influenced directly when it is introduced into the reactor, the uncontrolled ($\Delta I=\Delta F=0$) position and volume of the bubble have to be predicted using a predictor ($\hat{P}$). In this way the difference between the reference signal ($x(t)_{\mathrm{ref}}$) and the predicted signal ($\hat{x}(t)$) can be used to take the appropriate control action to reduce this difference. To

determine this control action, two methods can be used.

The control action of the first method is determined by simple multiplication of the (predicted) difference and the feedback weight matrix (K). The feedback weight matrix is calculated by inverting an overall approximate linear model describing the relation between the difference in volume (ΔV) and position (ΔZ) of the last bubble with $\Delta I{=}\Delta F{=}0$ and with the control actions ΔI and ΔF.

The second method does not use a single constant feedback matrix, instead it uses different matrices for each value of the reference signal. In general, the period (T) of the reference signal ($x(t)_{\mathrm{ref}}$) is longer than one bubble injection time (T_{p}), so $T{=}nT_{\mathrm{p}}$. Now a 'control section' is defined for integer values of n. This means that a period-4 reference signal has four control sections. For each of these control sections a separate linear model is used to describe the influence of the control actions on state (Z, V) of the just detached bubble. This second method allows an accurate description of the influence of the control actions on the state of the last bubble, since these influences themselves depend on the bubble's state.

Fig. 6(C) and (D) shows two examples of how the control actions (ΔI and ΔF) influence the bubble state. Fig. 6(C) and (D) are obtained by simulating the bubble state from the initial condition, corresponding to control section i, to the state corresponding to control section j, when $\Delta I{=}\Delta F{=}0$ and when ΔI and ΔF are allowed to vary within a range of $\pm 50\%$ of I_{o} and F_{o}, respectively.

When Fig. 6(C) and 6(D) are compared, it can be seen that the models used to describe the effect of the control actions on the bubble state, have to be different in both cases and are thus state-dependent. The discontinuity in Fig. 6(C) can be described using two separate models. Furthermore it appears difficult to describe the changes in position (ΔZ) and volume (ΔV) as function of ΔI and ΔF with an invertible linear model, since the slope of lines with constant ΔI in Fig. 6(D) depend on the value of ΔI itself. To overcome this problem, ΔI and ΔF are fitted directly as a function of ΔZ and ΔV, using a model that is linear in its parameters, but contains higher order terms in ΔZ, ΔV, and $\Delta Z{\times}\Delta V$; if the predicted ΔZ and ΔV are known, ΔI and ΔF can be calculated using these linear models.

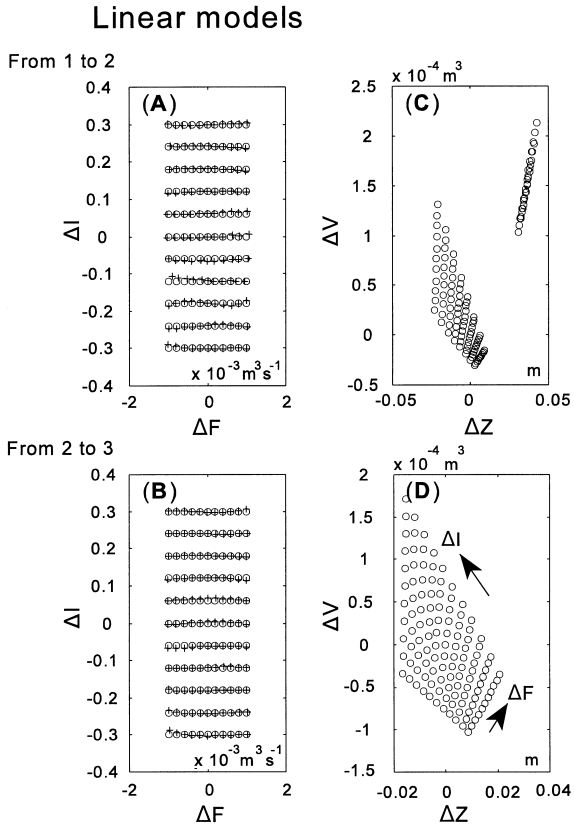

Fig. 6. Examples of linear models ((A), (B)) used to predict the control action as a function of the last bubble's state. The figures (A) and (B) show how ΔI and ΔF are predicted (+) from ΔZ and ΔV. The resemblance between the predicted (+) and imposed (○) control actions is satisfactory. The figures (C) and (D) show how the bubble's state (○) is changed due to the control actions used (○ in (A) and (B)).

In the next section different bubble patterns are stabilized using both the method with the constant feedback matrix and the method with the state-dependent feedback matrices. The effect of stabilizing these bubble patterns is shown by comparing conversion and selectivity of the ammoxidation of propylene in both the controlled and uncontrolled situations.

4. Results

Section 4.1 deals with the stabilization of different bubble patterns. In Section 4.2 the influence of the changed bubble dynamics on the propylene ammoxidation is shown.

Table 1
Parameter settings

Parameter	Value
W_{bed}	50×10^{-2} m
D_{bed}	4×10^{-2} m
F_o	2×10^{-3} m^3 s^{-1}
T_p	0.113 s
I_o	0.6

4.1. Stabilization of bubble patterns

The simulations of the bubble patterns by the dynamic bubble model were performed using the parameter values listed in Table 1. To find UPOs that could be used as reference signals (see Section 3.1), a time series was generated of states (viz., positions and volumes) of all the bubbles present in the reactor. The 'sample' time was taken equal to T_p. So each time a new bubble was initiated at the distributor, the state of the model was saved. In this time series, a number of low period (smaller than 10 times T_p), almost periodic, orbits was found by simply searching for $x(t+nT_p)\approx x(t)$, where $x(t)$ is the state of the last bubble.

First of all, two period-4 orbits were found (P4I, P4II). The first orbit, P4I was successfully controlled using a global linear model (constant feedback matrix, see Fig. 7I). It is clear that there is a significant difference between the reference signal ($*$) and the model itself ($\circ$). The result however, is a period-4 bubble pattern that resembles the one shown in Fig. 8 (P4III).

When the same method, using a constant feedback matrix, was tried for the second period-4 orbit (P4II), it failed. To cope with this, four state-dependent linear models, one for each control section, were determined. To avoid having to wait for the model to get synchronized with the signal generator, the simulation was started using an initial bubble pattern corresponding to the reference signal. Instead of a successful stabilization of a period-4 bubble pattern, a period-16 behavior was observed (Fig. 7II and Fig. 8 P4II). Finally, the period-4 orbit was stabilized when the simulation was started using a reactor without any bubbles as initial condition (Fig. 7III and Fig. 8 P4III).

This remarkable result, viz. stabilizing two different bubble patterns using the same reference signal but different initial conditions, may be explained by the low dimensionality of the reference signal. Control

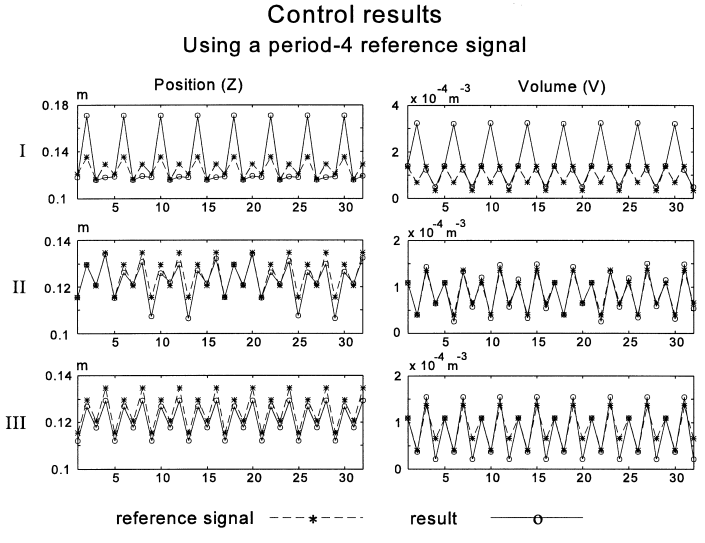

Fig. 7. Results using the period-4 reference signals. In situation I, P4I (Fig. 8) was used together with the global feedback matrix. In situations II and III, P4II (Fig. 8) was used as reference signal. In situation II the simulation was started with a bubble pattern corresponding to P4II, whereas in situation III no bubbles were present at the start of the simulation.

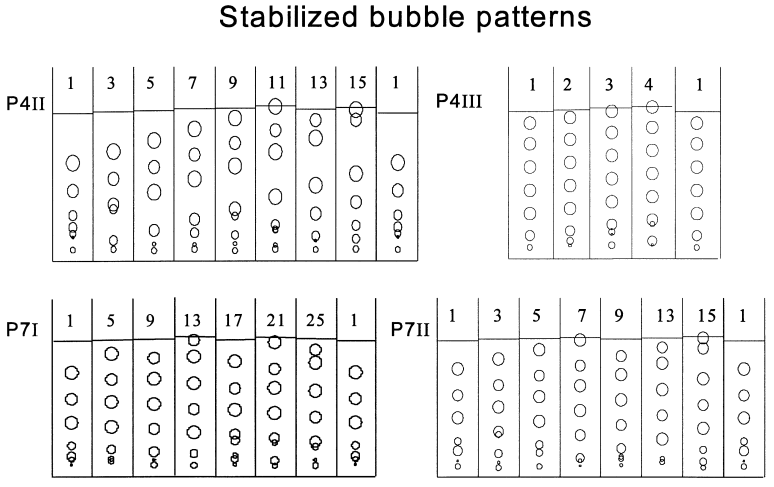

Fig. 8. Four of the five stabilized bubble patterns. P4I is omitted since it looks nearly the same as P4III (although the bubble sizes are different). P4II is the period-16 pattern. This pattern is clearly different from P4III. A group of three bubbles travels together and is then followed by a small empty space (no bubbles). P7I and P7II look similar to each other. At the 14th and 28th section a coalescing pair escapes, while at the 7th and 21st section a single bubble escapes.

actions are determined on the basis of *only* the state of the last bubble. Since typically seven to ten bubbles are present in the reactor, different initial conditions might give different periodic solutions.

Apart from the two period-4 orbits, also a number of period-7 orbits were found. Although there are slight differences between each of these period-7 orbits, they very much look the same; so they were averaged to give one period-7 orbit ($P7_m$). Again it was tried to speed up calculations by starting with an initial bubble pattern corresponding to the first control section of this orbit. However, this resulted in a period-28 orbit (Fig. 8 P7I). When the simulation was started with no bubbles in the reactor, no control could be achieved using $P7_m$ as a reference signal. However, control could be achieved when one of the original (instead of the average) period-7 orbits (P7II) was used as the reference signal. This resulted in a period-14 (Fig. 8 P7II) bubble pattern.

This last observation, that not the average but one of the original period-7 orbits results in a periodic bubble pattern, clearly shows the complexity and sensitivity of the dynamic bubble model. When the bubble patterns resulting from the period-7 reference signals are inspected, it seems reasonable that the bubble pattern is not period-7 but period-14 or 28 (Fig. 8 P7I and P7II). Up until about one third of the reactor height a 'bubble growth zone' is present. In this zone the bubble gets its final size. However, the period-7 reference signal leads to a smaller bubble trailed by a larger bubble. The larger bubble tries to overtake the smaller bubble thus creating a larger distance to the one below it. This results in an alternating pattern of two (nearly) coalesced bubbles leaving the reactor (control sections 14 and 28), followed by a single bubble (7 and 21). This is in contrast to the period-4 behavior in Fig. 8 P4III, where bubbles leave the 'bubble growth zone' with a uniform size.

4.2. Example of a catalytic reaction

The ammoxidation of propylene to acrilnitril (Sohio process) is schematically shown in Fig. 9. To simulate

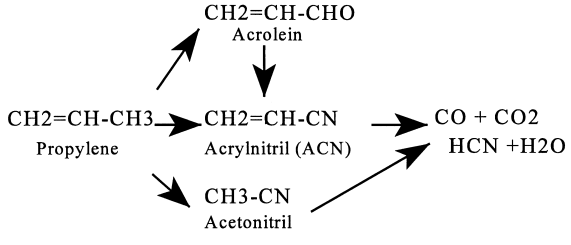

Fig. 9. Schematic representation of the propylene ammoxidation.

the effect of the changed bubble dynamics on the reactor's performance, the kinetic data reported by Hopper et al. [19] and Mleczko [20], is used. These data describe the reaction rate when reaction takes place on a Bi–Mo–O catalyst.

Using the kinetics and particle properties (d_p=100 μm) reported by Mleczko [20] this reaction is simulated in the reactor at 400°C. The maximum bubble injection flow is the same as reported in Table 1 at reactor conditions (2 l/s at 400°C). The other parameters listed in Table 1 are kept the same as well.

To compare the reactor performance of all five bubble patterns (cf., Fig. 8) with the uncontrolled reactor, the improvement or efficiency is defined as

$$\eta = \frac{Y_{\text{controlled}}}{Y_{\text{uncontrolled}}} - 1, \tag{1}$$

where Y is the yield of the desired product. This seems a reasonable definition of the improvement of the reactor performance. However, the total average flow of gas into the reactor may change due to the control actions (−10% to +10%). An improvement of the reactor performance might then be compensated by a decreased throughput (ΔV_o). To take this effect into account, an alternative definition of the improvement or efficiency is

$$\eta^* = \frac{(YF)_{\text{controlled}}}{(YF)_{\text{uncontrolled}}} - 1, \tag{2}$$

where F is the average bubble flow into the reactor. The simulation results are reported in Table 2. The results indicate clearly that a more uniform bubble pattern (viz., P4I and P4III) results in appreciably higher conversion, selectivity, and yields.

Table 2
Simulation results

	Base	p4I	p4II	p4III	p7I	p7II
x (%)	30.18	33.17	30.03	32.25	32.49	33.57
S (%)	54.80	56.63	55.38	56.96	55.53	55.42
Y (%)	16.54	18.78	16.63	18.37	18.04	18.60
ΔV_o (%)	0	−3.28	+2.76	+1.24	−5.06	−8.77
η (%)	0	13.5	0.5	11.1	9.1	12.5
η^* (%)	0	9.8	3.3	12.4	3.6	2.6

5. Concluding remarks and future work

In this paper, a model is presented, that is a dynamic extension of the simple classic two-phase reactor models used to predict chemical performance (i.e., conversion and selectivity) of fluidized bed reactors. The most important part of the model is the dynamic bubble model that can correctly predict bubble sizes and also exhibits chaotic dynamics. By application of an extended version of Pyragas' control algorithm, the bubble dynamics can be changed from chaotic to periodic in a 'flow' regime, in which the model otherwise would predict a chaotic bubble behavior.

The potential improvement of the chemical performance, as expressed in improvements upto 12.4% is a considerable stimulation to look for an experimental implementation of this or a similar chaos control method. Future work will focus on this experimental implementation. In a number of steps the control scheme of Fig. 5 will be implemented. First of all, an appropriate measured variable has to be found. One could think of (differential) pressure measurements and/or optical signals giving information about bubble positions and sizes. Furthermore, a 'process model' is needed (e.g. a neural net) to predict future values of the measured variable and to calculate the necessary control actions (i.e., change in bubble gas flow) to manipulate the future values towards the desired trajectory.

6. Notation

A	bubble mass transfer area (m^2)
C_b	bubble phase concentration (mol m^{-3})
C_e	emulsion phase concentration (mol m^{-3})
D_{bed}	bed thickness (m)
F_b	bubble injection flow (m^3 s^{-1})
$F_{b,ij}$	bubble flow from i to j (m^3 s^{-1})
F_{mf}	minimum fluidization flow (m^3 s^{-1})
F_o	maximum bubble flow (m^3 s^{-1})
H_f	fluidization height (m)
H_{mf}	height at minimum fluidization (m)
I_o	on-fraction of the bubble flow (dimensionless)
K	mass transfer coefficient (m s^{-1})
R_i	radius of bubble i (m)
S	selectivity (dimensionless)

T_p	bubble injection period (s)
U_i	bubble rise velocity (m s^{-1})
$U_{i\infty}$	single bubble rise velocity (m s^{-1})
U_{mf}	minimum fluidization velocity (m s^{-1})
V_i	volume of bubble i (m^3)
V_e	compartment emulsion volume (m^3)
V_b	compartment bubble volume (m^3)
W_{bed}	width of the fluid bed reactor (m)
X	conversion (dimensionless)
$x(t)$	measured variable(s) [x]
$x(t)_{ref}$	generated reference signal [x]
Y	yield (dimensionless)
Z_i	vertical position of bubble i (m)
ΔF	control action on maximum bubble flow ($m^3 s^{-1}$)
ΔI	control action on 'on-fraction' (dimensionless)
ΔV	predicted deviation in volume (m^3)
ΔV_o	average deviation in initial bubble volume (m^3)
ΔZ	predicted deviation in position (m)
$\phi_{i\rightarrow j}$	volume exchange between bubbles i and j (m^3 s^{-1})
η	improvement based on yield (dimesionless)
η^*	improvement based on throughput (dimensionless)

Acknowledgements

The investigations were supported (in part) by the Netherlands Foundation for Chemical Research (SON) as part of the SON programme 'Young Chemists' with financial aid from the Netherlands Organization for Scientific Research (NWO). The authors are grateful to Prof. Dr. F. Takens for the valuable discussions during development of the bubble model and control scheme.

References

[1] J.R. Postrup-Nielsen, Chem. Eng. Sci. 50(24) (1995) 4061.
[2] J.R. Postrup-Nielsen, Catal. Today 22 (1994) 295.
[3] K. Takacs, H.P. Calis, A.W. Gerritsen, C.M. van den Bleek, Chem. Eng. Sci. 51(10) (1996) 1789.
[4] K.R. Westerterp, Chem. Eng. Sci. 47 (1992) 2195.
[5] J.C. Schouten, M.L.M. van der Stappen, C.M. van den Bleek, Chem. Eng. Sci. 51(10) (1996) 1991.
[6] M.L.M. van der Stappen, Chaotic hydrodynamics of fluidized beds, Ph.D. Thesis, TU Delft, 1996.
[7] J.K. Beeckmans, K. MacWilliam, Powder Technol. 45(2) (1986) 177.
[8] J.C. Orcutt, J.F. Davidson, R.L. Pigford, AIChE Symp. Ser. 58(38) (1962) 1.
[9] D. Kunii, O. Levenspiel, Ind. Eng. Chem. Res. 29 (1990) 1226.
[10] R. Clift, J.R. Grace, AIChE Symp. Ser. 66(105) (1970) 14.
[11] R. Clift, J.R. Grace, AIChE Symp. Ser. 67(116) (1971) 23.
[12] R. Clift, J.R. Grace, in: J.F. Davidson, R. Clift, D. Harrison (Eds.), Fluidization, Academic Press, London, 1985, p. 73.
[13] C.S. Daw, J.S. Halow, AIChE Symp. Ser. 88(289) (1992) 61.
[14] L.R. Glicksman, W.K. Lord, in: J.R. Grace, J.M. Matsen (Eds.), Proceedings of International Conference on Fluidization, Plenum Press, New York, 1980, p. 125.
[15] R.C. Darton, R.D. LaNauze, J.F. Davidson, D. Harrison, Trans. IChemE 55 (1977) 274.
[16] T. Kapitaniak, Controlling Chaos. Theoretical and Practical Methods in Non-linear Dynamics, Academic Press, London, 1996.
[17] T. Shinbrot, Adv. Phys. 44(2) (1995) 73.
[18] K. Pyragas, Phys. Lett. A 170 (1992) 421.
[19] J.R. Hopper, C.L. Yaws, T.C. Ho, M. Vichailak, Waste Management 13 (1993) 3.
[20] L. Mleczko, Chem. Technik 48(3) (1996) 130.
[21] P. Geuzens, D. Thoenes, Chem. Eng. Commun. 67 (1988) 717.